3711

Simultaneous and Robust Estimation of Cardiac-Induced 3D Brain Velocity and Diffusion Tensor Fields in the Human Brain

Kulam Najmudeen Magdoom[1,2,3], Alexandru V. Avram[1], Joelle Sarlls[4], and Peter J. Basser[1]
[1]Eunice Kennedy Shriver National Institute of Child Health and Human Development, National Institutes of Health, Bethesda, MD, United States, [2]The Military Traumatic Brain Injury Initiative (MTBI2), Uniformed Services University of the Health Sciences, Bethesda, MD, United States, [3]The Henry M Jackson Foundation for the Advancement of Military Medicine (HJF) Inc., Bethesda, MD, United States, [4]National Institute of Neurological Disorders and Stroke, National Institutes of Health, Bethesda, MD, United States

Synopsis

Keywords: Quantitative Imaging, Neuro

Motivation: Cardiac-induced brain pulsation is crucial for brain function, yet its measurement is challenging due to small displacements.

Goal(s): The goal of this study is to develop a robust method to simultaneously measure both the cardiac-induced brain velocity vector and the corresponding diffusion tensor fields.

Approach: We acquire DWIs with long diffusion times to enhance flow sensitivity and employ an outlier rejection method to eliminate inconsistent phase signals. Velocity vector and diffusion tensor fields were estimated from phase and magnitude images, respectively.

Results: The high variability in the velocities across acquisitions was significantly reduced using our approach. The brain appeared still during late diastole.

Impact: This study facilitates the measurement of intrinsic brain tissue motion with heartbeat compared to DENSE approaches, providing a new method for studying brain function.

Introduction

The pulsation of the brain with every heartbeat plays an important role in normal and abnormal functioning of the brain [1-3]. Cardiac pulsation can also corrupt/confound diffusion tensor imaging (DTI) [4] data which is thought to be broadly remediated with cardiac gating [5]. Phase contrast MRI with sub-voxel displacement sensitivity is an ideal method for imaging coherent displacements, however measuring subtle brain tissue motion (< 0.2 mm/s) can be confounded by unwanted phase contributions from other sources such as eddy currents and unpredictable head motion. In this study, we developed a new methodology to reliably and simultaneously measure both the diffusion tensor and 3D velocity vector fields associated with the brain motion as a function of the cardiac phase.

Methods

MRI data was acquired in three healthy young adults on a 3T scanner (Prisma, Siemens Healthineers) with 80 mT/m peak gradient strength and a 200 T/m/s slew rate using 20-channel coil. Whole-brain displacement encoded MRI data was acquired along the six directions of the icosahedron at b = 350 s/mm^2 and venc = 0.4 mm/s along with a b = 0 s/mm^2 scan using the following parameters: δ\Δ = 7\48 ms, FOV=210 x 210 x 120 mm, GRAPPA acceleration factor = 2, TR\TE = 5,600\71 ms, NEX = 144, and a 2 mm isotropic spatial resolution. The long diffusion time and short diffusion gradient pulse duration were chosen to increase flow sensitivity while the gradient strengths were adjusted to maintain adequate diffusion sensitivity [6]. The photoplethysmograph (PPG) signal and MRI triggers were simultaneously recorded using a Biopac System (Biopac, Goleta, CA, USA) for retrospective gating.

Phase images from all scans were unwrapped and registered to the corresponding magnitude images using FSL software [6]. The linear phase errors arising from eddy currents, head motion, etc., were removed using linear regression. The displacement encoded images were then segmented into eight different bins each 210 ms long covering the entire cardiac cycle. Multiple repetitions of the data acquired in each bin for a given direction were utilized to reject inconsistent phase measurement in each voxel. The consistent data were then averaged to estimate the 3D velocity vector and the diffusion tensor fields using linear regression of their phase and magnitude, respectively [4, 6].

Results and Discussion

The results obtained in a representative subject are shown in this section given their similarity with the other two subjects. The accuracy of our approach is demonstrated by comparing the x-component (left-right) of the velocity at various cardiac phases obtained with and without outlier rejection as shown in Figure 1. It can be observed that the discontinuities in the velocity across the cardiac phases shown using arrows in the figure are removed with outlier rejection. The precision of our approach is shown in Figure 2 using the three components of the velocity obtained in the second cardiac bin where the discrepancy was observed in Figure 1. In each subject, multiple runs derived from oversampled data were nearly indistinguishable. The 3D velocity vector field across the cardiac phases are shown in Figure 3. The funnel shaped motion of the brain along its superior-inferior axis well known in literature [8, 9] is captured in these plots. It can also be observed that the brain appears still only in late diastole (> 75% RR interval) indicating there may be an effect of cardiac pulsation related brain movement in cardiac gated DTI acquisitions with typical trigger delays. Finally, diffusion tensor maps are shown in Figure 4 as a function of the cardiac phase. It can be observed that subtle changes in mean diffusivity (MD) and fractional anisotropy (FA) occur in regions with high brain tissue deformation as shown by the arrows. The MD increased with deformation as also shown in previous phantom studies [10, 11]. The FA also increased due to the anisotropic nature of the deformation field.

Conclusion

We have demonstrated an accurate and precise method to map the 3D velocity vector and diffusion tensor fields simultaneously in the human brain. The results show that brain tissue deforms continuously during most of the cardiac cycle. Our results suggest that cardiac gating may be necessary in DTI acquisitions when aiming to measure subtle changes in diffusion properties that often occurs in disease in brain regions with larger velocities.

Acknowledgements

This study was supported by the Intramural Research Program of the NICHD and NINDS. This work was also partly funded the Department of Defense in the Military Traumatic Brain Injury Initiative under award, HU0001-22-2-0058. The authors have no conflicts of interest to disclose. The views, information or content, and conclusions presented do not necessarily represent the official position or policy of, nor should any official endorsement be inferred on the part of, the Uniformed Services University, the Department of Defense, the U.S. Government or the Henry M. Jackson Foundation for the Advancement of Military Medicine, Inc.

References

1. Iliff, J. J., Wang, M., Zeppenfeld, D. M., Venkataraman, A., Plog, B. A., Liao, Y., ... & Nedergaard, M. (2013). Cerebral arterial pulsation drives paravascular CSF–interstitial fluid exchange in the murine brain. Journal of Neuroscience, 33(46), 18190-18199.
2. Wirestam, R., Salford, L. G., Thomsen, C., Brockstedt, S., Persson, B. R. R., & Ståhlberg, F. (1997). Quantification of low-velocity motion using a navigator-echo supported MR velocity-mapping technique: application to intracranial dynamics in volunteers and patients with brain tumours. Magnetic resonance imaging, 15(1), 1-11.
3. Hofmann, E., Warmuth-Metz, M., Bendszus, M., & Solymosi, L. (2000). Phase-contrast MR imaging of the cervical CSF and spinal cord: volumetric motion analysis in patients with Chiari I malformation. American Journal of Neuroradiology, 21(1), 151-158.
4. Basser, P. J., Mattiello, J., & LeBihan, D. (1994). MR diffusion tensor spectroscopy and imaging. Biophysical journal, 66(1), 259-267.
5. Chung, S., Courcot, B., Sdika, M., Moffat, K., Rae, C., & Henry, R. G. (2010). Bootstrap quantification of cardiac pulsation artifact in DTI. Neuroimage, 49(1), 631-640.
6. Magdoom, K. N., Zeinomar, A., Lonser, R. R., Sarntinoranont, M., & Mareci, T. H. (2019). Phase contrast MRI of creeping flows using stimulated echo. Journal of Magnetic Resonance, 299, 49-58.
7. Jenkinson, M., Beckmann, C. F., Behrens, T. E. J., Woolrich, M. W. & Smith, S. M. FSL. NeuroImage 62, 782–790 (2012).
8. Poncelet, B. P., Wedeen, V. J., Weisskoff, R. M., & Cohen, M. S. (1992). Brain parenchyma motion: measurement with cine echo-planar MR imaging. Radiology, 185(3), 645-651.
9. Sloots, J. J., Biessels, G. J., & Zwanenburg, J. J. (2020). Cardiac and respiration-induced brain deformations in humans quantified with high-field MRI. Neuroimage, 210, 116581.
10. Nevo, U., Özarslan, E., Komlosh, M. E., Koay, C. G., Sarlls, J. E., & Basser, P. J. (2010). A system and mathematical framework to model shear flow effects in biomedical DW-imaging and spectroscopy. NMR in Biomedicine, 23(7), 734-744.
11. Reese, T. G., Wedeen, V. J., & Weisskoff, R. M. (1996). Measuring diffusion in the presence of material strain. Journal of Magnetic Resonance, Series B, 112(3), 253-258.

Figures

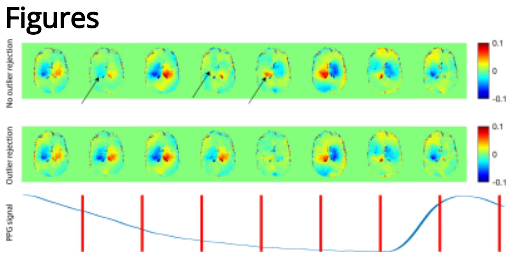

Figure 1: The effect of outlier rejection on the velocity estimation. The x-component (left-right) of mean velocity vector (mm/s) obtained with and without outlier rejection. The recorded PPG signal is shown in the third row with the 210 ms bins indicated by red bar. Differences in estimated velocity between the two approaches are shown using arrows.

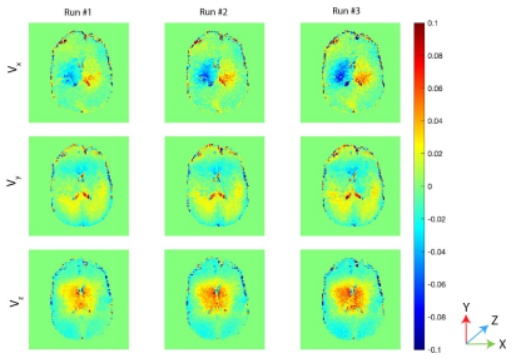

Figure 2: Precision of our approach shown using the velocity vector map obtained in the second cardiac bin for the three repetitions (i.e., runs) on each subject obtained using the extra samples collected. The components of the velocity vector (mm/s) are shown as rows while the repetitions are shown along the columns. The coordinate system is shown on the right corner for reference. It can be observed that the three runs were nearly indistinguishable.

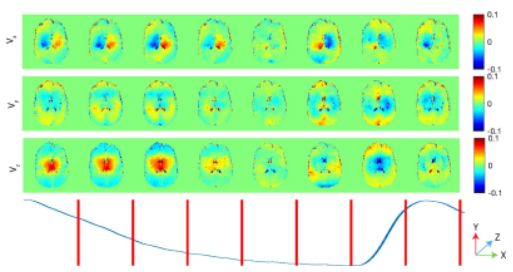

Figure 3: The 3D velocity vector (mm/s) in the brain over different segments of the cardiac cycle. The three components of the velocity vector are shown in the first three rows. A representative PPG waveform with bins indicated by red bars is shown in the bottom row. The coordinate system is shown in the right corner for reference. It can be observed that all components of the velocity vector are negligible only in late diastole.

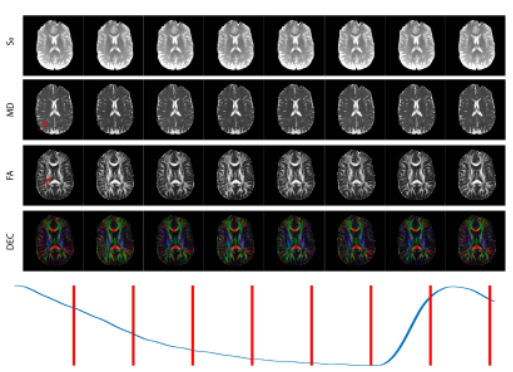

Figure 4: The measured diffusion tensor in the brain as a function of the cardiac phase. (First row) non-diffusion weighted image (S0), (Second row) Mean diffusivity (MD) given by the trace of the diffusion tensor, (Third row) Fractional anisotropy (FA), (Fourth row) Direction encoded color (DEC). A representative PPG cycle with segments shown using red bars. Subtle changes in FA and MD in select brain regions are shown using arrows.

Proc. Intl. Soc. Mag. Reson. Med. 32 (2024)
3711